Spatially Resolved Electrochemistry in Ionic Liquids: Surface Structure Effects on Triiodide Reduction at Platinum Electrodes

Barak D.B. Aaronson,[†] Stanley C.S. Lai,[†,‡] and Patrick R. Unwin[†,]*

† Department of Chemistry, University of Warwick, Gibbet Hill Rd, CV4 7AL, Coventry, UK

‡ *MESA+ Institute for Nanotechnology, University of Twente, PO Box 217, 7500 AE Enschede, The Netherlands.*

ABSRACT:

Understanding the relationship between electrochemical activity and electrode structure is vital for improving the efficiency of dye-sensitized solar cells. Here, the reduction of triiodide to iodide in 1-butyl-3-methylimidazolium tetrafluoroborate ([BMIm][BF_4]) room temperature ionic liquid (RTIL) is investigated on polycrystalline platinum using scanning electrochemical cell microscopy (SECCM) and correlated to the crystallographic orientation from electron backscatter diffraction (EBSD). Although the rate determining step in all grains was the first electron transfer, significant grain-dependent variations in activity were revealed, with grains with a dominant (110) crystallographic character exhibiting higher catalytic activity compared to those with a major (100) orientation. The SECCM technique is demonstrated to resolve heterogeneity in activity, highlighting that methods incorporating

polycrystalline electrodes miss vital details for understanding and optimizing electrocatalysts. An additional advantage of the SECCM over single crystal techniques is its ability to probe high index facets.

I. INTRODUCTION

Dye sensitized solar cells (DSSCs) have attracted widespread attention as a low cost alternative to conventional solar cells since the seminal report by O'Regan and Grätzel in the early 90s.[1,2] Typically, a DSSC consists of a dye-sensitized TiO_2 photo-electrode and a platinum counter electrode (CE) that sandwich an organic electrolyte solution containing a redox shuttle. The processes at the sensitized electrode are photo-excitation and electron injection followed by oxidation of the dye. The oxidized form of the dye is then regenerated by the redox shuttle, which is reduced at the CE. Although alternatives to platinum as the CE material[3] and the triiodide (I_3^-) / iodide (I^-) redox couple[4] as the mediator have been suggested, these remain the most common components.[5] However, compared to other processes occurring in DSSCs, there are relatively few mechanistic studies of the reduction of I_3^- to I^- at platinum in various media.[6-9] In this paper we show that the rate of this reaction in room temperature ionic liquids (RTILs) is strongly influenced by the local structure of the Pt electrodes and identify the optimal surface for electrocatalysis.

DSSCs typically employ acetonitrile[2] as the organic electrolyte, but there is now considerable interest in using RTILs[10,11] owing to their low vapor pressure, high stability, low toxicity and wide potential window. Although there have been previous macroscale studies on the I_3^-/I^- redox couple at polycrystalline Pt electrodes in RTILs,[8,12] such studies prevent an understanding of structural and dimensional effects that may significantly influence electrocatalytic activity.[13-17] This is particularly important for the process of I_3^- reduction at Pt, since strong dependences of the kinetics on the size and morphology of Pt particles have

been reported in acetonitrile.[18-20] As photoelectrodes become more efficient, there will be a need to ensure that cell efficiencies do not become limited by CE processes.

Here we show how scanning electrochemical cell microscopy (SECCM)[21,22] can be used to image electrode reaction rates in RTILs that are correlated with local electrode structure (via electron backscatter diffraction (EBSD)). This represents a major new environment for SECCM which has, hitherto, been used only for aqueous electrolyte/electrode interfaces, albeit with some success.[13,23] RTILs have generally proven challenging for probe imaging techniques, due to the high viscosity and (for electrochemical probe methods) low (and widely different) diffusion coefficients of redox species.[24-26] In contrast, we have found that RTILs can be used readily for SECCM.

2. EXPERIMENTAL

For the present studies the SECCM tip and sample were deployed in a custom-built environmental chamber in which dry nitrogen gas (N_2) was flowed to facilitate the removal of dissolved oxygen as well as to assist in drying of the droplet at the end of the probe (Figure 1).[27] Full details are provided in the Supporting Information (SI) section S1. In brief, a dual barrel glass capillary pulled to a fine tip (1.6 μm diameter) was filled with a solution of interest (10 mM triiodide solution in RTIL). The RTIL used, was 1-butyl-3-methylimidazolium tetrafluoroborate [BMIm][BF_4]). (≥ 97.0 % purity, (HPLC grade), Sigma Aldrich) and was used fresh without further treatment. The 10 mM I_3^- solution was prepared by dissolving equimolar amounts of I_2 (98 % purity, Fischer Chemicals) and tetrabutylammonium iodide (TBAI) (98 % purity, Acros Organics) in the RTIL, leaving the solution in a sealed vial in an ultrasonic bath for 2 hrs. Both barrels of the SECCM tip were filled quickly with the RTIL solution using a nonmetallic syringe needle (MicroFil). Ag wire

(0.255 mm 3N, MaTeck), rinsed with water and then ethanol, followed by drying under a nitrogen flow was used as quasi-reference/counter electrodes (QRCEs). An Ag QRCE was inserted into each barrel and a bias potential was applied between the two QRCEs to establish an ion conductance current across the meniscus at the end of the pipet, which was monitored. An oscillation (amplitude ~ 200 nm peak to peak) was applied to the probe in the *z* direction, leading to an alternating current (AC) component of the ionic conductance signal, i_C, due to the periodical compression and expansion of the meniscus at the end of the pipet while in contact with the surface.

The substrate of interest (polycrystalline platinum foil, purity > 99.95 %, 0.0125 mm thickness; Advent Research Materials) was flame-annealed prior to experiments and connected as a working electrode (WE) with an area defined by the size of the meniscus contact (roughly the size of the pipet, corresponding to ~ 2-3 × 10^{-8} cm^2).

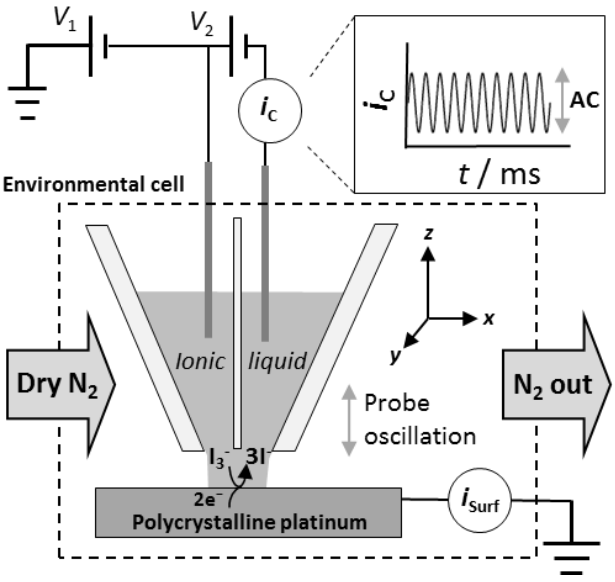

Figure 1. Schematic of the SECCM setup, employing a dual barrel glass pipet pulled to a fine tip (1.6 μm diameter). A bias potential (V_2) of + 0.2 V was applied between two Ag QRCEs and the conductance current (i_C) was monitored to provide positional feedback (normal to the

surface). The working electrode potential ($V_{Surf} = -V_1 - V_2/2$)) was varied by changing V_1 and the resulting surface current (i_{Surf}) was recorded.

Electron backscatter diffraction (EBSD) images of platinum substrates were recorded on a Zeiss SUPRA 55 variable-pressure field emission scanning electron microscope (FE-SEM) at 20 kV on a 70° tilted sample with an EDAX TSL EBSD system, after the SECCM scans. EBSD images were constructed from diffraction patterns recorded every 1 µm. The samples were rinsed with deionized water before insertion into the vacuum chamber of the EBSD.

II. RESULTS AND DISCUSSION

At relatively low concentrations, triiodide (I_3^-) is formed through the equilibrium between iodine (I_2) and iodide (I^-), which lies to the right in organic solvents and ionic liquids. The redox reactions of interest herein are:[7]

$$3\ I_2 + 2\ e^- \leftrightarrows\ 2\ I_3^- \qquad (1)$$

$$I_3^- + 2\ e^- \leftrightarrows 3\ I^- \qquad (2)$$

Reaction 2 has been described to proceed via a complex mechanism in both acetonitrile[7] and in RTILs[28] but there is some consensus[13-15,29] that the reaction may proceed on platinum via:

$$I_{3\,(sol)}^- \leftrightarrows I_{2(sol)} + I^- \qquad (3)$$

$$I_{2(sol)} + 2\ * \leftrightarrows 2\ I^* \qquad (4)$$

$$2\ I^* + 2\ e^- \leftrightarrows 2\ I^- \qquad (5)$$

where * denotes the free site on the electrode surface and sol denotes the solution phase.

Cyclic voltammograms (CVs) were recorded in the SECCM setup (meniscus contact) and a typical CV is shown in Figure 2. Starting at + 0.6 V *vs.* Ag QRCE and sweeping in the

cathodic direction, the reduction of I_3^- is observed with an apparent onset potential of + 0.5 V. Changing sweep direction at - 0.1 V, I^- is oxidized back to I_3^- and starting at + 0.65 V , I_3^- is further oxidized to form I_2. The CV in the SECCM setup is characterized by relatively fast mass transport rates, such that interfacial kinetic effects are manifested in the CVs (*vide infra*).

To estimate the formal potential for reaction 2 in [BMIm][BF_4], macroscale CVs were recorded, yielding an apparent formal potential of + 0.51 (± 0.03) V vs. AgQRE (see SI section S2) at low potential sweep rates, consistent with values in the literature.[9] This value was confirmed by open circuit potential measurements of equimolar concentrations of I_3^- and I^- in [BMIm][BF_4] (SI, section S2).

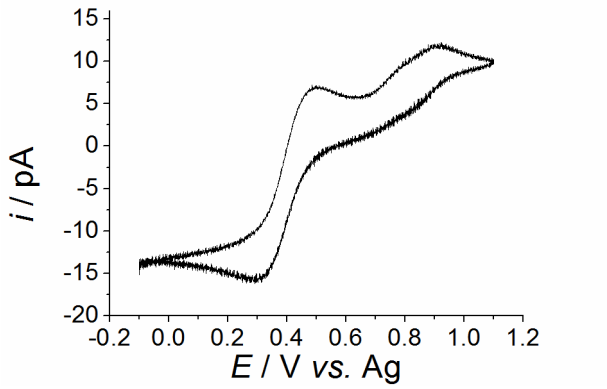

Figure 2. SECCM cyclic voltammogram of 10 mM I_3^- in [BMIm][PF_4] on polycrystalline platinum foil. Scan rate of 100 mV s^{-1}.

SECCM images (Figure 3) were acquired at different electrode potentials for the I^-/I_3^- process, ranging between + 0.45 V and + 0.30 V. The pipet scan rate was set so that a characteristic residence time (meniscus diameter/pipet scan rate) of 3 seconds was achieved, ensuring that a steady-state response was established (see SI, section S1). As depicted in Figures 3(a) - (d), the average (steady-state) reduction current increases from *ca.* 1.5 pA at +

0.45 V to *ca.* 12 pA at + 0.30 V, in good agreement with the reduction wave in the CV in Figure 2 (taking account of its transient nature). Notably, significant variations in surface current are observed across the SECCM images, with the current changing by more than a factor of two between well-defined regions of low and high activity. A crystallographic orientation map of the same area, obtained with EBSD (Figure 3e), reveals a strong correlation between individual crystallographic grains and the variations in the SECCM surface current maps, highlighting significant electrode structural dependency of the kinetics of the I^-/I_3^- process.

SECCM acquires other maps simultaneously with the surface current image: topography, direct current (DC) conductance and the AC component of the conductance current between the barrels in the probe (Figure 1),[21] used as a feedback parameter to maintain a constant tip-substrate separation (meniscus height) throughout a scan.[22] The DC and AC components of the conductance current are highly sensitive to changes in wetting and droplet shape.[21,22,30] A typical AC amplitude map (set-point value of 20 pA), shown in Figure 3f, verifies the stability of the RTIL meniscus droplet during the SECCM scan. Most importantly, this stability indicates that the electrochemical variations seen in Figures 3(a) - (d) are not due to a change in droplet size and are essentially due to variations in inherent activity. However, in proximity to grain boundaries there appear to be some small perturbation of the droplet, leading to a change in the AC value that can be used to highlight the granular structure of the sample (Figure 3(f) and Figure 4(a)). This effect verifies the spatial correlation found between the SECCM images and EBSD map, as grain boundaries are highlighted by both imaging techniques and can be used as a means of self-referencing between images as well as to provide a precise estimate for the meniscus size (Figure 4(b)). In addition, we have previously shown, using atomic force microscopy (AFM) that there is

similar roughness of individual grains on such polycrystalline platinum foils[13] excluding the possibility of significant differences in wetting between individual grains.

A key feature of SECCM is that we can estimate the magnitude of any ohmic drop via the conductance current between the two QRCEs. This is gained from analysis of the DC conductance current maps, such as the example shown in Figure 4(a). The DC conductance maps, exhibited a steady DC of *ca.* 3 nA (corresponding to a resistance at the tip of *ca.* 66 MΩ for a bias potential of +0.2 V) throughout the scan with minute (but detectable) variations at grain boundaries. The ohmic drop (*i*R) associated with the tip resistance during scanning is negligible and accounts for less than a 1 mV when calculated for the highest currents observed (~ - 14 pA in Figure 3(d)), highlighting the strength of the SECCM technique over macroscopic measurements.

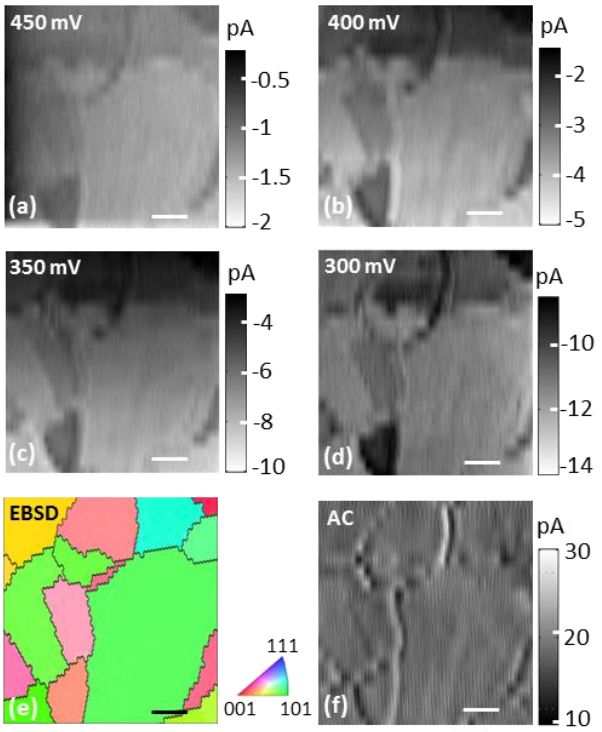

Figure 3. SECCM and EBSD maps of a Pt electrode. (a) – (d) Spatially resolved surface currents for the reduction of 10 mM I_3^- in [BMIm][BF_4] at 450, 400, 350 and 300 mV *vs.* Ag QRCE, respectively. (e) EBSD image of the scanned area, black lines between grains are to guide the eye. (f) Typical AC amplitude ion conductance map during the scan at 400 mV (illustrating the general uniformity of the AC feedback over grains, while highlighting grain boundaries). Scale bar in all images is 10 μm.

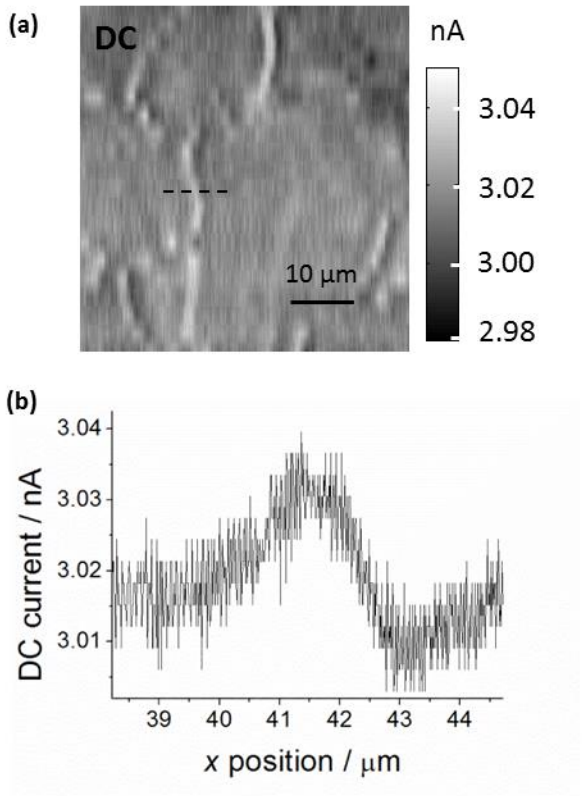

Figure 4 – SECCM DC conductance map at an electrode potential of + 0.4 V**.** (a) Typical DC conductance map in the SECCM setup exhibiting highly stable values around 3 nA. The bias voltage between the QRCEs was + 0.2 V. (b) Cross section of the dotted line in (a) where the meniscus contact area was estimated as < 3 μm in diameter (*i.e.* of the order of the probe size) where the DC was perturbed the most (at grain boundaries, shown in Figure 3(e)).

Inspection of the EBSD image (Figure 3(e)) and surface electrochemical images (Figures 3(a) - (d)) indicates that individual grains with a high contribution of the (110) orientation correlate to higher reduction currents at all potentials, whereas grains with a high contribution of the (100) orientation lead to lower reduction currents. The latter observation is in agreement with recent studies of hydrogen oxidation on basal plane Pt electrodes in RTILs,[31] where the surface adsorption of the anion ($[BF_4^-]$) was considered to possibly impede electrocatalysis. The decreased activity for less compact surfaces (Pt (100)) was related to the stronger anion adsorption compared to more densely packed crystalline planes,

Pt (110) and Pt (111). Similar trends in activity have been observed in preferentially-shaped nanoparticles in acetonitrile.[19]

To give a qualitative comparison of the variations in activity between grains, effective exchange current densities (j^0) were calculated. A Tafel analysis of the four images in Figure 3 was performed (see SI section S3) yielding values of spatially-resolved j^0 values and apparent Tafel slopes for the scanned area of the Pt foil. These are shown as images in Figure 5(a) and 5(b), respectively.

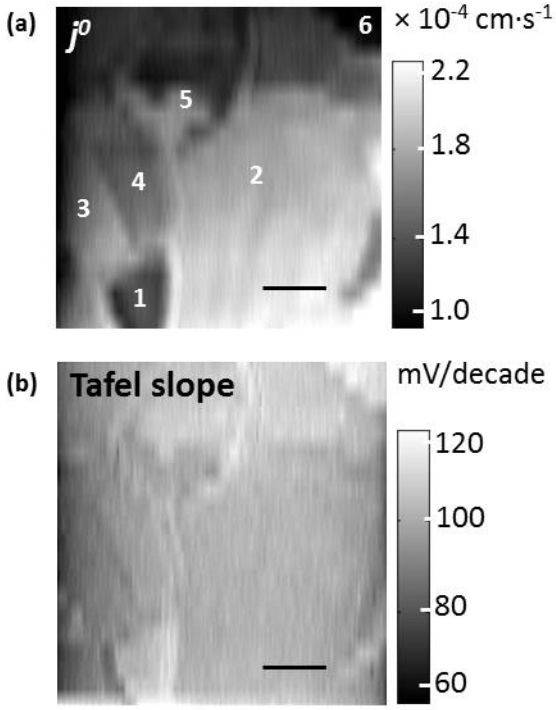

Figure 5. Tafel analysis of SECCM images. (a) Spatially resolved exchange current densities (j^0) values for the reduction of I_3^- from the analysis of SECCM images. Several well-defined grains are numbered. (b) Spatially resolved Tafel slope analysis of the area in (a). Scale bar in (a) and (b) is 10 μm.

The variation in effective j^0 is between 1.8 (± 0.3) × 10^{-4} cm·s^{-1}, for the more active grains (e.g. 2, 3 and 5 in Figure 5(a)) and 0.9 (± 0.1) × 10^{-4} cm·s^{-1} for the less active grains (e.g. 1 and 6 in Figure 5(a)). Figures 3 and 5 highlight key information from SECCM on spatially resolved ET kinetics that is lost in macroscale measurements involving polycrystalline platinum electrodes. Figure 5(b) shows that the apparent Tafel slopes display little variation across the surface (see also Figure S2 in SI), with all grains between 100 and 120 mV per decade, suggesting that the rate determining step[6,8,29] in the mechanism in all grains is the first electron transfer (nominally 120 mV per decade).

III. CONCLUSION

In the context of DSSCs, this study reveals that the rate of the I_3^- reduction process at the (polycrystalline) CE is structure-dependent and is influenced by the subtle variations in crystallographic orientation of the electrode. Pt CEs with more (110) character will improve the activity of the process. The unique advantage of SECCM over single crystal measurements is the ability to investigate high index facets which are difficult to obtain, but are ubiquitous in practical applications.

This study has also opened up spatially resolved measurements of fundamental electrochemical and electrocatalytic processes in RTILs, which are of considerable (and growing) interest for many important applications in energy technologies, electrosynthesis and sensing. As shown in this paper, SECCM is able to resolve variations in surface activity that are missed in conventional macro-scale techniques and, furthermore, through the use of complementary microscopy and structural techniques, is able to readily identify the best surfaces for optimal (electro)catalysis with the advantage of being able to probe high index facets.

ASSOCIATED CONTENT

SECCM, Macroscale CVs, SECCM Tafel analysis. This material is available free of charge via the Internet at http://pubs.acs.org.

AUTHOR INFORMATION

Corresponding Author

* p.r.unwin@warwick.ac.uk

Notes

The authors declare no competing financial interest.

ACKNOWLEDGMENT

This project was supported by the European Research Council through Advanced Investigator Grant ERC-2009-AdG 247143; "QUANTIF". SCSL was further supported by a Marie Curie Intra-European Fellowship within the EU's PF7 Program (project no. 275450; "VISELCAT"). The authors thank Dr. Kim McKelvey for fruitful discussion on data analysis, Dr. Maxim Joseph for contributions to sample preparation, Mr. Anatolii Cuharuc and Dr. Dimitry Momotenko for fruitful discussions, Ms. Changhui Chen for expert advice on EBSD analysis and Mr. Lee Butcher and Mr. Marcus Grant for providing parts for the experimental setup. We appreciate the expert design of custom electronics by Dr. Alex Colburn.

REFERENCES

(1) O'Regan, B.; Grätzel, M. A low-cost, high efficiency solar cell based on dye-sensitized colloidal TiO_2 films *Nature* **1991**, *353*, 737-740.

(2) Hagfeldt, A.; Boschloo, G.; Sun, L. C.; Kloo, L.; Pettersson, H. Dye-Sensitized Solar Cells *Chem. Rev.* **2010**, *110*, 6595-6663.

(3) Wu, M.; Lin, X.; Wang, Y.; Wang, L.; Guo, W.; Qi, D.; Peng, X.; Hagfeldt, A.; Grätzel, M.; Ma, T. Economical Pt-Free Catalysts for Counter Electrodes of Dye-Sensitized Solar Cells *J. Am. Chem. Soc.* **2012**, *134*, 3419-3428.

(4) Nusbaumer, H.; Moser, J.-E.; Zakeeruddin, S. M.; Nazeeruddin, M. K.; Grätzel, M. $Co^{II}(dbbip)_2^{2+}$ Complex Rivals Tri-iodide/Iodide Redox Mediator in Dye-Sensitized Photovoltaic Cells *J. Phys. Chem. B* **2001**, *105*, 10461-10464.

(5) Boschloo, G.; Hagfeldt, A. Characteristics of the Iodide/Triiodide Redox Mediator in Dye-Sensitized Solar Cells *Acc. Chem. Res.* **2009**, *42*, 1819-1826.

(6) Nakata, R.; Okazaki, S.; Fujinaga, T. Polarographic behavior of iodine in non-aqueous solvents *J. Electroanal. Chem.* **1981**, *125*, 413-420.

(7) Macagno, V. A.; Giordano, M. C.; Arvía, A. J. Kinetics and mechanisms of electrochemical reactions on platinum with solutions of iodine-sodium iodide in acetonitrile *Electrochim. Acta* **1969**, *14*, 335-357.

(8) Rogers, E. I.; Silvester, D. S.; Aldous, L.; Hardacre, C.; Compton, R. G. Electrooxidation of the Iodides $[C_4mim]I$, LiI, NaI, KI, RbI, and CsI in the Room Temperature Ionic Liquid $[C_4mim][NTf_2]$ *J. Phys. Chem. C* **2008**, *112*, 6551-6557.

(9) Zhang, Y.; Zheng, J. B. Investigation on the electro-oxidation of iodide in the room temperature ionic liquid, 1-butyl-3-methylimidazolium tetrafluoroborate at platinum electrode *Electrochim. Acta* **2007**, *52*, 4082-4086.

(10) Hapiot, P.; Lagrost, C. Electrochemical Reactivity in Room-Temperature Ionic Liquids *Chem. Rev.* **2008**, *108*, 2238-2264.

(11) Quinn, B. M.; Ding, Z.; Moulton, R.; Bard, A. J. Novel Electrochemical Studies of Ionic Liquids *Langmuir* **2002**, *18*, 1734-1742.

(12) Ejigu, A.; Lovelock, K. R. J.; Licence, P.; Walsh, D. A. Iodide/triiodide electrochemistry in ionic liquids: Effect of viscosity on mass transport, voltammetry and scanning electrochemical microscopy *Electrochim. Acta* **2011**, *56*, 10313-10320.

(13) Aaronson, B. D. B.; Chen, C.-H.; Li, H.; Koper, M. T. M.; Lai, S. C. S.; Unwin, P. R. Pseudo-Single-Crystal Electrochemistry on Polycrystalline Electrodes: Visualizing Activity at Grains and Grain Boundaries on Platinum for the Fe^{2+}/Fe^{3+} Redox Reaction *J. Am. Chem. Soc.* **2013**, *135*, 3873-3880.

(14) Narayanan, R.; El-Sayed, M. A. Shape-Dependent Catalytic Activity of Platinum Nanoparticles in Colloidal Solution *Nano Lett.* **2004**, *4*, 1343-1348.

(15) Koper, M. T. M. Structure sensitivity and nanoscale effects in electrocatalysis *Nanoscale* **2011**, *3*, 2054-2073.

(16) Tian, N.; Zhou, Z.-Y.; Sun, S.-G.; Ding, Y.; Wang, Z. L. Synthesis of Tetrahexahedral Platinum Nanocrystals with High-Index Facets and High Electro-Oxidation Activity *Science* **2007**, *316*, 732-735.

(17) Oja, S. M.; Wood, M.; Zhang, B. Nanoscale Electrochemistry *Anal. Chem.* **2012**, *85*, 473-486.

(18) Bönnemann, H.; Khelashvili, G.; Behrens, S.; Hinsch, A.; Skupien, K.; Dinjus, E. Role of the Platinum Nanoclusters in the Iodide/Triiodide Redox System of Dye Solar Cells *J. Cluster Sci.* **2007**, *18*, 141-155.

(19) Zhang, B.; Wang, D.; Hou, Y.; Yang, S.; Yang, X. H.; Zhong, J. H.; Liu, J.; Wang, H. F.; Hu, P.; Zhao, H. J.; Yang, H. G. Facet-Dependent Catalytic Activity of Platinum Nanocrystals for Triiodide Reduction in Dye-Sensitized Solar Cells *Sci. Rep.* **2013**, *3*.

(20) Somik, M.; Balavinayagam, R.; Griggs, L.; Hamm, S.; Baker, G. A.; Fraundorf, P.; Sengupta, S.; Shubhra, G. Ultrafine sputter-deposited Pt nanoparticles for triiodide reduction

in dye-sensitized solar cells: impact of nanoparticle size, crystallinity and surface coverage on catalytic activity *Nanotechnology* **2012**, *23*, 485405.

(21) Ebejer, N.; Güell, A. G.; Lai, S. C. S.; McKelvey, K.; Snowden, M. E.; Unwin, P. R. Scanning Electrochemical Cell Microscopy: A Versatile Technique for Nanoscale Electrochemistry and Functional Imaging *Annu. Rev. Anal. Chem.* **2013**, *6*, 329-351.

(22) Snowden, M. E.; Güell, A. G.; Lai, S. C. S.; McKelvey, K.; Ebejer, N.; O'Connell, M. A.; Colburn, A. W.; Unwin, P. R. Scanning Electrochemical Cell Microscopy: Theory and Experiment for Quantitative High Resolution Spatially-Resolved Voltammetry and Simultaneous Ion-Conductance Measurements *Anal. Chem.* **2012**, *84*, 2483-2491.

(23) Lai, S. C. S.; Patel, A. N.; McKelvey, K.; Unwin, P. R. Definitive Evidence for Fast Electron Transfer at Pristine Basal Plane Graphite from High-Resolution Electrochemical Imaging *Angew. Chem. Int. Ed.* **2012**, *51*, 5405-5408.

(24) Ghilane, J.; Lagrost, C.; Hapiot, P. Scanning Electrochemical Microscopy in Nonusual Solvents: Inequality of Diffusion Coefficients Problem *Anal. Chem.* **2007**, *79*, 7383-7391.

(25) Walsh, D. A.; Lovelock, K. R. J.; Licence, P. Ultramicroelectrode voltammetry and scanning electrochemical microscopy in room-temperature ionic liquid electrolytes *Chem. Soc. Rev.* **2010**, *39*, 4185-4194.

(26) Carano, M.; Bond, A. M. Prospects for the Application of Scanning Electrochemical Microscopy in Ionic Liquids *Aust. J. Chem.* **2007**, *60*, 29-34.

(27) Zhao, C.; Bond, A. M.; Compton, R. G.; O'Mahony, A. M.; Rogers, E. I. Modification and Implications of Changes in Electrochemical Responses Encountered When Undertaking Deoxygenation in Ionic Liquids *Anal. Chem.* **2010**, *82*, 3856-3861.

(28) Bentley, C. L.; Bond, A. M.; Hollenkamp, A. F.; Mahon, P. J.; Zhang, J. Concentration and electrode material dependence of the voltammetric response of iodide on

platinum, glassy carbon and boron-doped diamond in the room temperature ionic liquid 1-ethyl-3-methylimidazolium bis(trifluoromethanesulfonyl)imide *Electrochim. Acta* **2013**, *109*, 554-561.

(29) Hauch, A.; Georg, A. Diffusion in the electrolyte and charge-transfer reaction at the platinum electrode in dye-sensitized solar cells *Electrochim. Acta* **2001**, *46*, 3457-3466.

(30) Lai, S. C. S.; Dudin, P. V.; Macpherson, J. V.; Unwin, P. R. Visualizing Zeptomole (Electro)Catalysis at Single Nanoparticles within an Ensemble *J. Am. Chem. Soc.* **2011**, *133*, 10744-10747.

(31) Navarro-Suárez, A. M.; Hidalgo-Acosta, J. C.; Fadini, L.; Feliu, J. M.; Suárez-Herrera, M. F. Electrochemical Oxidation of Hydrogen on Basal Plane Platinum Electrodes in Imidazolium Ionic Liquids *J. Phys. Chem. C* **2011**, *115*, 11147-11155.